Organic & Biomolecular Chemistry

Accepted Manuscript

ROYAL SOCIETY OF CHEMISTRY

www.rsc.org/obc

Control of Reaction Pathways in the Photochemical Reaction of a Quinone with Tetramethylethylene by Metal Binding

Hiroaki Yamamoto,[a] Kei Ohkubo,[b] Seiji Akimoto,[c] Shunichi Fukuzumi[b] and Akihiko Tsuda*[a]

[a] Department of Chemistry, Graduate School of Science, Kobe University, 1-1 Rokkodai-cho, Nada-ku, Kobe 657-8501, Japan

[b] Department of Material and Life Science, Graduate School of Engineering, Osaka University, ALCA, Japan Science and Technology Agency, Suita, Osaka 565-0871, Japan

[c] Molecular Photoscience Research Center, Kobe University, 1-1 Rokkodai-cho, Nada-ku, Kobe 657-8501, Japan

E-mail: tsuda@harbor.kobe-u.ac.jp

Abstract

The present study reports a novel supramolecular photochemical reaction that focuses on the direct electronic interactions between a host reaction substrate and guest metal salts. The reaction pathways in the photochemical reactions of quinone derivatives bearing a methoxy group and a long oligoether sidearm $\mathbf{QE_n}$ (n = 0 and 3) with tetramethylethylene (TME) are changed upon noncovalent complexations of the host reactant with alkali and alkaline earth metal ions and a transition metal salt. The photochemical reaction of $\mathbf{QE_n}$ with TME provides a mixture of [2+2] cycloadducts $\mathbf{1aE_n}$ and $\mathbf{1bE_n}$, hydroquinone $\mathbf{H_2QE_n}$, and monoallyl ether adducts of hydroquinone $\mathbf{2aE_n}$ and $\mathbf{2bE_n}$. The photochemical reaction proceeds by the photoinduced electron transfer mechanism, where photoirradiation brings about formation of a radical ion pair [$\mathbf{QE_n}^{\bullet-}$, $\mathrm{TME}^{\bullet+}$] as the primary intermediate. We found

that the yields and selectivity of these photoproducts are changed upon electronic interactions of $\mathbf{QE_n}^{\bullet-}$ with the metal salts. The photochemical reaction in the absence of metal salt provides $\mathbf{H_2QE_n}$ as its major product, whereas $\mathbf{QE_3}$, having the long sidearm, dominantly produces $\mathbf{2aE_3}$ at the expense of $\mathbf{1aE_3}$, $\mathbf{1bE_3}$, and $\mathbf{H_2QE_3}$, when it forms a size-favorable host–guest complex with divalent Ca^{2+}. In contrast, $\mathbf{QE_n}$ selectively provides oxetanes $\mathbf{1aE_n}$ and $\mathbf{1bE_n}$ in the presence of $Pd(OAc)_2$, which can form complexes with the quinone through metal–olefin and coordination interactions in the ground and photoexcited states of the quinone.

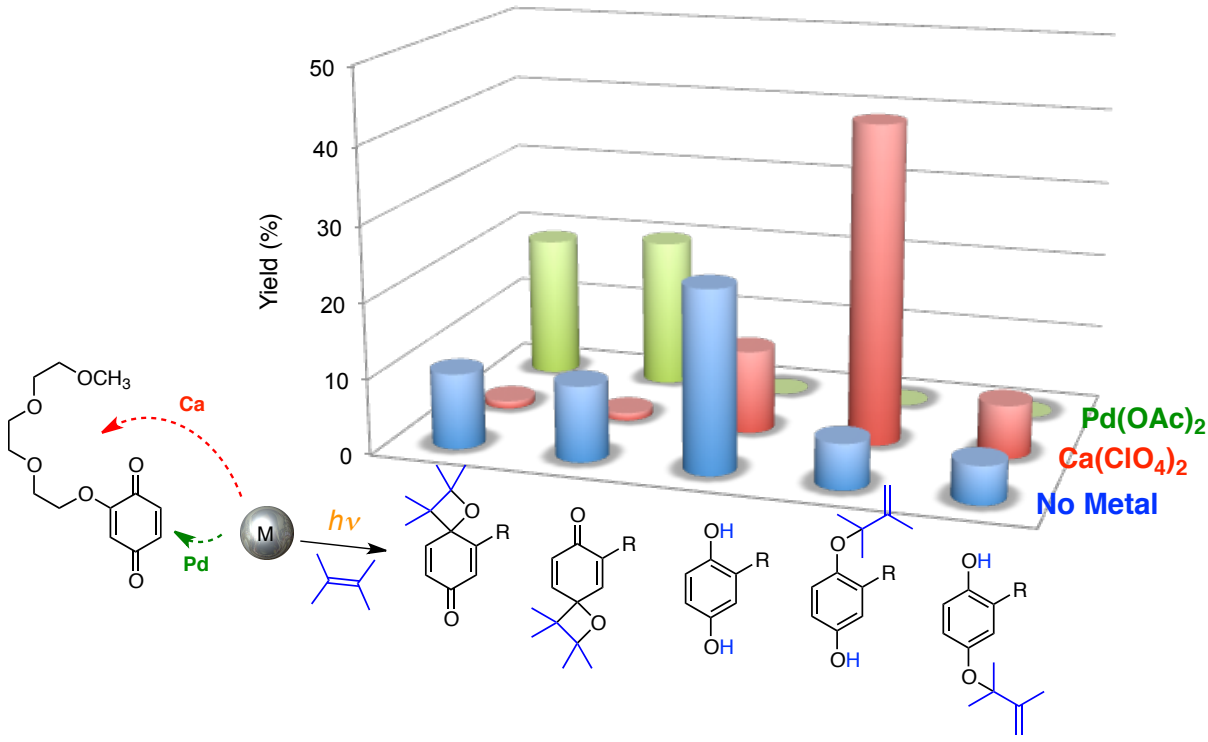

Introduction

Photochemical synthesis is a complementary method of synthesizing molecules that are difficult to obtain through thermal reactions. Precise control of the photochemical reaction is, however, more difficult to achieve than that of the thermal reaction, because the excited states are short-lived with high reactivity even at low temperatures. In general, steric and electronic modifications of the reactant molecule result in change in reaction pathways of the

photochemical reactions. On the other hand, supramolecular photochemical reactions occur by accommodation of the reactant molecules in the confined cavities of the host molecules[1–13] or by noncovalent binding with the template molecule or metal.[14–17] The host and the template allow specific reactions of the reactant molecules with highly restricted structures and orientations in the molecular assemblies (Figure 1a). However, less attention has been paid to the direct electronic interactions between the host and guest, especially for those that can be seen in the noncovalently linked metal–host complexes.[18]

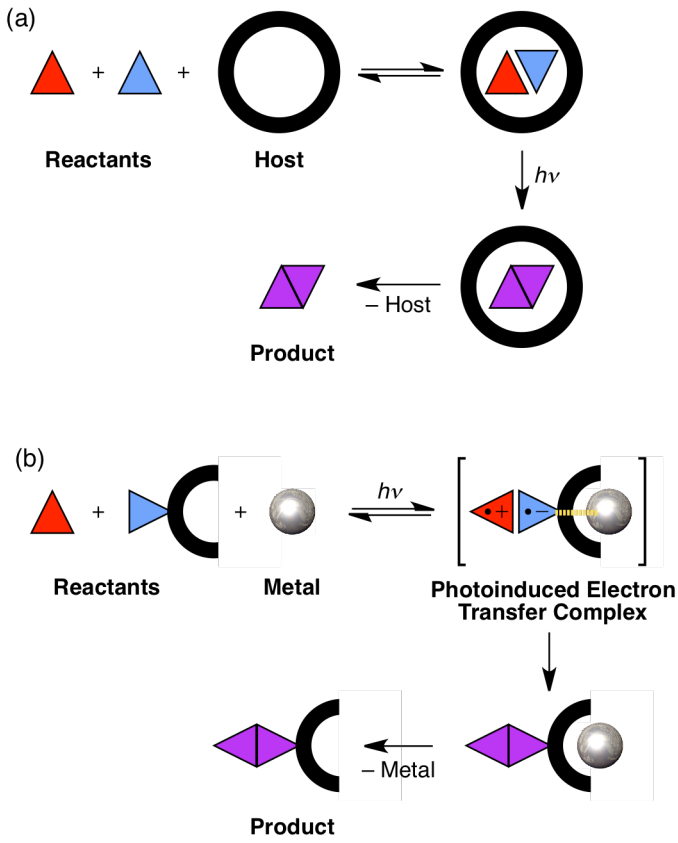

Figure 1. Concepts of supramolecular photochemical reactions through (a) inclusion of reactants in a host cavity, and (b) metal binding of the photoinduced electron transfer complex.

One of the authors reported a metal-catalyzed photochemical reaction, where a magnesium ion promotes the photochemical reaction of organosilane with an aromatic

carbonyl compound that proceeds through a photoinduced electron transfer mechanism.[19] Mg^{2+}–carbonyl interaction exhibited a remarkable increase in the redox reactivity of carbonyl compounds.[20] On the other hand, Kochi and coworkers reported a salt–inhibited photochemical reaction, where tetra-*n*-butylammonium hexafluorophosphate suppresses the [2+2] cycloaddition of *p*-chloranil with stilbene that also proceeds through a photoinduced electron transfer mechanism.[21] The added salt interacts with the intermediate radical ion pair by ion exchange to separate the *p*-chloranil anion and the stilbene cation. Subsequently, we hypothesized that a strong site-selective metal binding by the reaction substrate itself in the photoinduced electron transfer reaction dramatically changes the photochemical reaction pathways (Figure 1b).[22] Such control of the photochemical reaction pathways by strong metal–host interactions has yet to be reported.

Scheme 1. 2-Substituted Quinones $\mathbf{QE_0}$ and $\mathbf{QE_3}$, and Their Metal-Complexations in the Ground State.

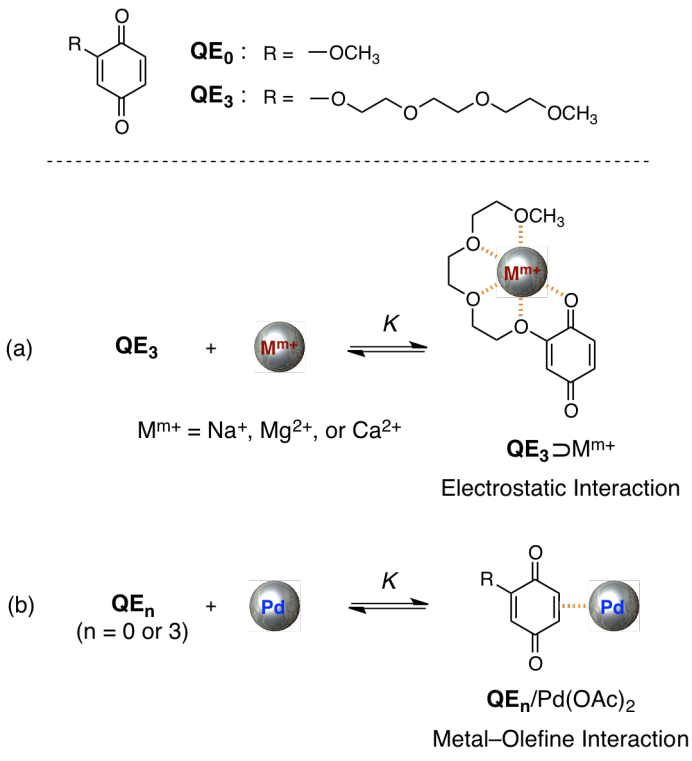

There are some reports for thermal supramolecular reactions using the noncovalent metal complexes as the reaction substrate.[23,24] We previously reported that a quinone derivative **QE$_3$** (Scheme 1), bearing a long oligoether sidearm, dramatically accelerates [4+2] cycloaddition with cyclopentadiene upon noncovalent complexation with metal ion.[23] This is an example of the thermal supramolecular reaction,[24–27] where the bound metal ion lowers LUMO of the quinone with respect to the HOMO of cyclopentadiene. We herein anticipated that **QE$_3$** can form metal complexes with the oligoether and/or quinone moiety in both the ground and photoexcited states, which change the photoinduced electron transfer reaction pathways by steric and electronic interactions.

It is known that the photochemical reaction of a quinone with olefin provides [2+2] adducts such as cyclobutane and oxetane.[28] The reactions forming the later oxetane usually proceed through the photoinduced electron transfer mechanism, being called Paterno–Büchi reactions.[29,30] Oshima and coworkers reported that photochemical reaction of *p*-benzoquinone with TME gave not only the oxetane but also monoallylethers of hydroquinone in the photoinduced electron transfer mechanism (Scheme 2).[31] With our hypothesis described above, photochemical reactions of **QE$_n$** (n = 0 or 3) with tetramethylethylene (TME) have been examined in the absence and presence of metal ions (Na^+, Mg^{2+}, Ca^{2+}, and transition metal salt of $Pd(OAc)_2$). We have found that the product selectivity of oxcetanes, hydroquinone, and monoallylether of hydroquinones and the quantum yield are changed by complexations of **QE$_n$** and the readical anions (**QE$_n^{\bullet-}$**) with the metal salts in the course of the photochemical reactions. The binding modes of metal salts with **QE$_n^{\bullet-}$** is clarified by the direct detection of the metal salts complexes by ESR spectroscopy.

Scheme 2. Photochemical Reaction of *p*-Benzoquinone with TME.

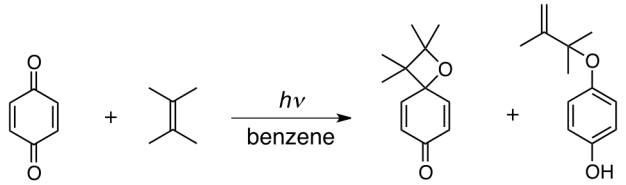

^{1}H NMR Spectroscopy of QE_3 with or without Metal Salts.

Although $\mathbf{QE_0}$ in the ground state rarely forms metal complexes with alkaline metal and alkaline earth metal ions in MeCN, $\mathbf{QE_3}$ bearing a long oligoether sidearm can form the metal complexes.[23] $\mathbf{QE_3}$, having a podand-type structure, forms size-favorable complexes with Na^+ and Ca^{2+} with the binding constant K = 120 and 4900 M^{-1}, respectively, in 1:1 stoichiometry at 20 °C, but forms a size-mismatch complex with the smaller Mg^{2+} with a relatively lower binding constant K = 69 M^{-1} (Table 1 and Figure S1). Representatively, ^{1}H NMR spectrum of $\mathbf{QE_3}$ in CD_3CN exhibited large downfield shifts (Figure 2a and 2b) upon complexation with Ca^{2+}. The signals observed at δ = 4.1–3.3 and 6.8–6.0 ppm, corresponding to the oligoether sidearm and quinone moiety, respectively, showed downfield shifts with $\Delta\delta$ = 0.19–0.29 and 0.20–0.22 ppm, respectively. These observed peak shifts indicate that Ca^{2+} binds $\mathbf{QE_3}$ at its carbonyl group and oligoether sidearm, where the guest Ca^{2+} strongly withdraws electrons through oxygen atoms (Scheme 1a).[32]

Table 1. Photochemical Reactions of $\mathbf{QE_3}$ with TME in the Absence or Presence of Metal Salt.[a]

Entry	Metal Salt [b]	Yield (%) [c]					K (M^{-1}) [d]	E_{red} vs Fc^+/Fc (V)	ΔG_{ET} (kcal mol^{-1}) [e]	Quantum Yield (Φ) [g]
		$\mathbf{1aE_3}$	$\mathbf{1bE_3}$	$\mathbf{H_2QE_3}$	$\mathbf{2aE_3}$	$\mathbf{2bE_3}$				
1	None	10	10	24	6	5		–0.81	–10.9	0.21
2	$NaClO_4$	5	11	33	17	8	120	–0.62	–17.8 [f]	0.24
3	$Mg(ClO_4)_2$	9	8	26	21	5	69	*h*	*h*	0.27
4	$Ca(ClO_4)_2$	1	1	11	42	7	4900	–0.18	–28.2 [f]	0.32
5	$Pd(OAc)_2$	19	20	–	–	–	*h*	–0.83	–7.1 [f]	0.06

[a] MeCN solution containing 10 mM of $\mathbf{QE_3}$ and 40 mM of TME (4 eq.) without or with metal salt upon photoirradiation at λ > 420 nm at 20 °C. [b] Metal salt concentration and reaction time: 100 mM and 20 min for $NaClO_4$, $Mg(ClO_4)_2$, $Ca(ClO_4)_2$, and 10 mM and 150 min for $Pd(OAc)_2$. [c] Determined by HPLC and ^{1}H NMR. [d] Determined at 20 °C. [e] Calculated by using the Weller free energy relationship for photoinduced electron transfer (eq. 1). [f] Observed value. [g] Determined by ferrioxalate actinometry. [h] The value could not be determined.

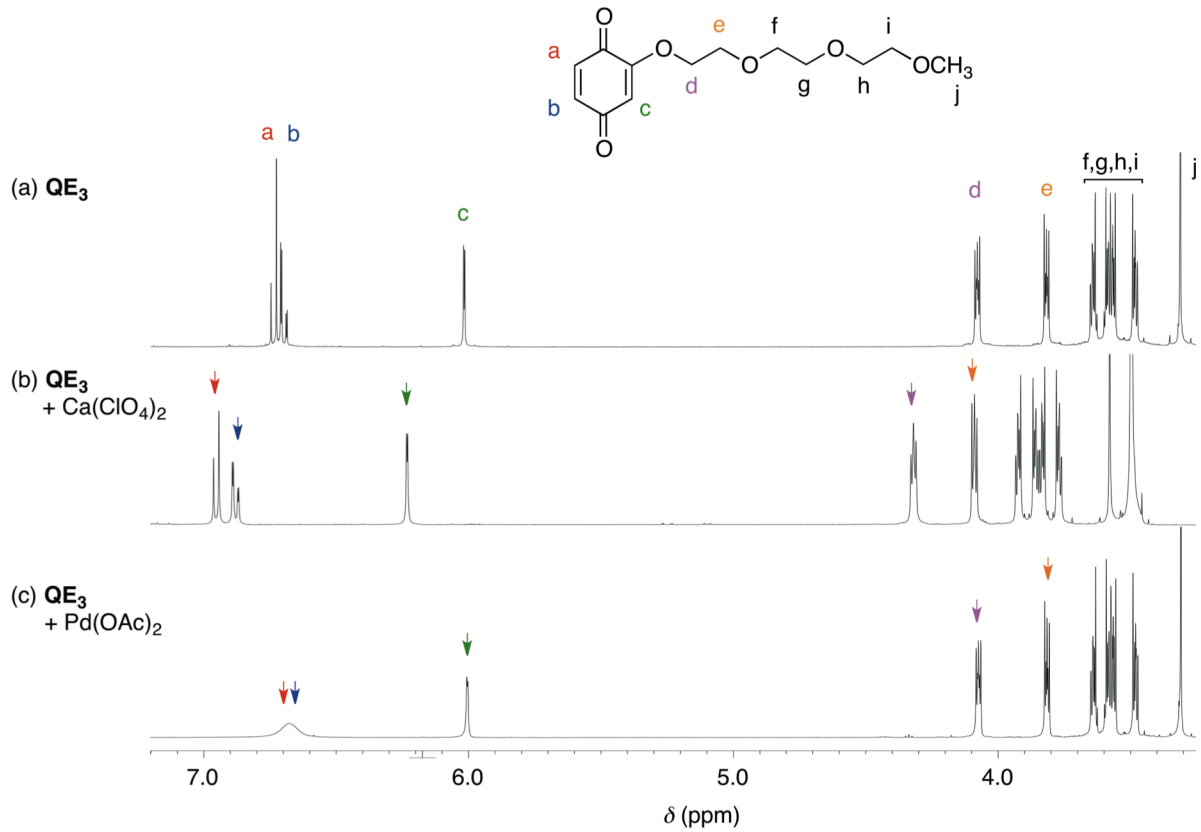

Figure 2. ^{1}H NMR spectral changes of **QE$_3$** upon mixing with metal salts in CD_3CN. (a) **QE$_3$**, (b) 1:3 mixture of **QE$_3$** and $Ca(ClO_4)_2$, and (c) 1:3 mixture of **QE$_3$** and $Pd(OAc)_2$. [**QE$_3$**] = 10 mM.

When **QE$_3$** was mixed with $Pd(OAc)_2$,[33] however, the two set of signals at δ = 6.69 and 6.73 ppm, corresponding to the vinyl protons of C5 and C6 positions, respectively, notably broaden into a unified single peak at δ = 6.67 ppm (Figure 2c). In sharp contrast, no notable change was observed in the other protons, including those in the oligoether sidearm. This characteristic peak shift suggests the formation of a metal–olefin complex at C5–C6 olefin (Scheme 1b).[34,35] The observed preference of the complexation at C5–C6 olefin rather than C2–C3 olefin can be explained by their different π-electronic structures and steric hindrance caused by the presence of either the methoxy or the oligoether group.[35] Since the metal–olefin complexation is usually very weak in the neutral state, we could not determine the binding constant between **QE$_3$** and $Pd(OAc)_2$. Although TME, having a double bond, is also expected to form an analogous palladium–olefin bond and/or π-allylpalladium complex,[36] its ^{1}H NMR

signal of methyl protons, observed at δ = 1.66 ppm, showed no change upon mixing with $Pd(OAc)_2$ in the same conditions (Figure S2). The four methyl groups of TME may sterically hinder the possible metal–olefin interaction. As expected, even in the 1:1:1 ternary mixture of **QE_3**, TME, and $Pd(OAc)_2$, **QE_3** showed the same spectral changes without changes of TME signals (Figure S3).

Redox Potentials of QE_3 in the Absence and Presence of Metal Salts.

The one-electron reduction potentials of **QE_3** in the absence and presence of metal salts in MeCN containing 0.1 M Bu_4NClO_4 as a supporting electrolyte were determined by cyclic voltammetry (Figure S4 and Table 1).[37] The cyclic voltammogram of **QE_3** showed the one-electron redox couple at $E_{1/2}$ = –0.81 V vs Fc/Fc^+, corresponding to **$QE_3/QE_3^{\bullet-}$**. In reference to *p*-benzoquinone, which provided the redox couple at $E_{1/2}$ = –0.70 V, the observed lower potential of **QE_3** indicates that the oligoether group attached at C2 position donates electrons to the quinone moiety. When $Ca(ClO_4)_2$, having the largest binding constant with **QE_3** in the series of metal ions, was added into the sample solution, a large positive shift ($\Delta E_{1/2}$ = +0.63 V) of the redox couple was observed. As indicated by the ^{1}H NMR spectroscopic study described above, Ca^{2+} significantly withdraws electrons from **QE_3** through electronic interactions with carbonyl and ether oxygens in the complex (Scheme 1a). The smaller positive shift of the reduction potential of **QE_3** was observed with monovalent Na^+ ($\Delta E_{1/2}$ = +0.19 V). Although Mg^{2+} also brought about a positive shift of the reduction potential, the redox profile becomes irreversible. In contrast, a very small negative shift of the redox ($\Delta E_{1/2}$ = –0.02 V) was observed without notable change of the redox profile of the quinone upon mixing with $Pd(OAc)_2$, having the irreversible reduction peak at around –0.52 V vs Fc/Fc^+.[38] This result indicates that $Pd(OAc)_2$ is electrically rather neutral for the one-electron redox process of the quinone. This agrees with the results obtained in ^{1}H NMR spectroscopic study, described above.

Photochemical Reactions of QE_n with TME.

When the photochemical reaction of $\mathbf{QE_0}$ with TME was performed in MeCN at 20 °C upon photoirradiation (>420 nm) for 20 min with a 500 W xenon lamp, a mixture of oxetanes $\mathbf{1aE_0}$ and $\mathbf{1bE_0}$, hydroquinone $\mathbf{H_2QE_0}$, and monoallyl ether adducts of hydroquinone $\mathbf{2aE_0}$ and $\mathbf{2bE_0}$ were obtained in 14, 17, 23, 3, and 5% yields, respectively (Scheme 3, entry 6 in Table 2, and Figure S5a). No notable change in the product yields was observed upon further photoirradiation of the sample solution. The products, isolated through the column chromatography or the preparative HPLC, were characterized by means of ^{1}H and ^{13}C NMR spectroscopy (see Supporting Information), IR spectroscopy, electrospray ionization (ESI) mass spectrometry, and elemental analysis. $\mathbf{2aE_0}$ was further characterized by X-ray crystallography (Figure S6).[39] In the reference reaction without TME, 40% decrease of $\mathbf{QE_0}$ was observed after photoirradiation for 20 min in both ^{1}H NMR spectroscopy and HPLC analysis (Figure S7). Since there was no detectable product in these analyses, $\mathbf{QE_0}$ may gradually decompose upon photoirradiation.

Scheme 3. Photochemical Reactions of $\mathbf{QE_n}$ with TME.

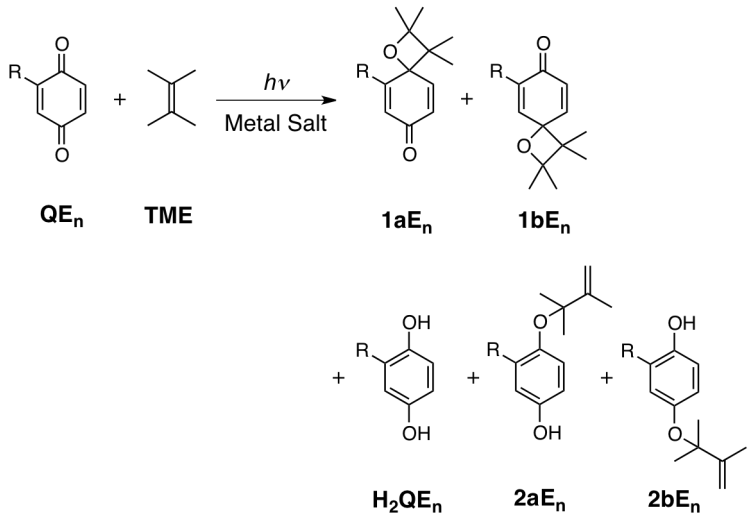

Table 2. Photochemical Reactions of $\mathbf{QE_0}$ with TME in the Absence or Presence of Metal Salt[a]

		Yield (%) [c]				
Entry	Metal Salt [b]	$\mathbf{1aE_0}$	$\mathbf{1bE_0}$	$\mathbf{H_2QE_0}$	$\mathbf{2aE_0}$	$\mathbf{2bE_0}$
6	None	14	17	23	3	5
7	$NaClO_4$	12	13	27	4	5
8	$Mg(ClO_4)_2$	10	11	21	11	2
9	$Ca(ClO_4)_2$	6	5	20	19	3
10	$Pd(OAc)_2$	22	27	–	–	–

[a] MeCN solution containing 10 mM of $\mathbf{QE_0}$ and 40 mM of TME (4 eq.) without or with metal salt upon photoirradiation at $\lambda > 420$ nm at 20 °C. [b] Metal salt concentration and reaction time: 100 mM and 20 min for $NaClO_4$, $Mg(ClO_4)_2$, $Ca(ClO_4)_2$, and 10 mM and 150 min for $Pd(OAc)_2$. [c] Determined by HPLC and ^{1}H NMR.

The free energy change for electron transfer (ΔG_{ET}) from TME to $^3\mathbf{QE_0}$* is estimated to be –8.1 kcal mol^{-1} by Weller equation (eq 1) using the reduction potential of $\mathbf{QE_0}$ (E_{red} =

$$\Delta G_{ET} \text{ (in eV)} = e(E_{ox} - E_{red}) - {}^3E(T)^* + w_p \quad (1)$$

–0.81 V vs Fc$^+$/Fc), the one-electron oxidation potential of TME (E_{ox} = 1.21 V) (Figure S8),[40] the triplet excitation energy of $\mathbf{QE_0}$ ($^3E(T)^*$ = 2.36 eV), which is evaluated from its phosphorescence spectrum with λ_{max} at 525 nm taken at 77 K (Figure S9), and the working term (w_p) is neglected in polar MeCN.[41-43] This result indicates that the photochemical reaction proceeds by the photoinduced electron transfer mechanism in which the photoirradiation brings about formation of the radical ion pair [$\mathbf{QE_0}^{\bullet-}$, $TME^{\bullet+}$] as the primary reaction intermediate, which then allows a biradical formation (path A), a proton transfer (PT) reaction (path B), and a hydrogen transfer (HT) reaction (path C) (Scheme 4a).[28–30,44] The path A provides oxetanes $\mathbf{1aE_0}$ and $\mathbf{1bE_0}$, while the paths B and C give hydroquinone $\mathbf{H_2QE_0}$ and monoallyl ether of hydroquinones $\mathbf{2aE_0}$ and $\mathbf{2bE_0}$. After the PT reaction in path B, the final products are produced through hydrogen transfer (HT) and radical coupling reactions of the tertiary allyl radical with the semiquinone radical (4-$\mathbf{HQE_0}^{\bullet}$ or 1-$\mathbf{HQE_0}^{\bullet}$). On the other hand,

Scheme 4. Reaction Pathways of $\mathbf{QE_n}$ with TME in the Absence and Presence of Ca^{2+} and $Pd(OAc)_2$

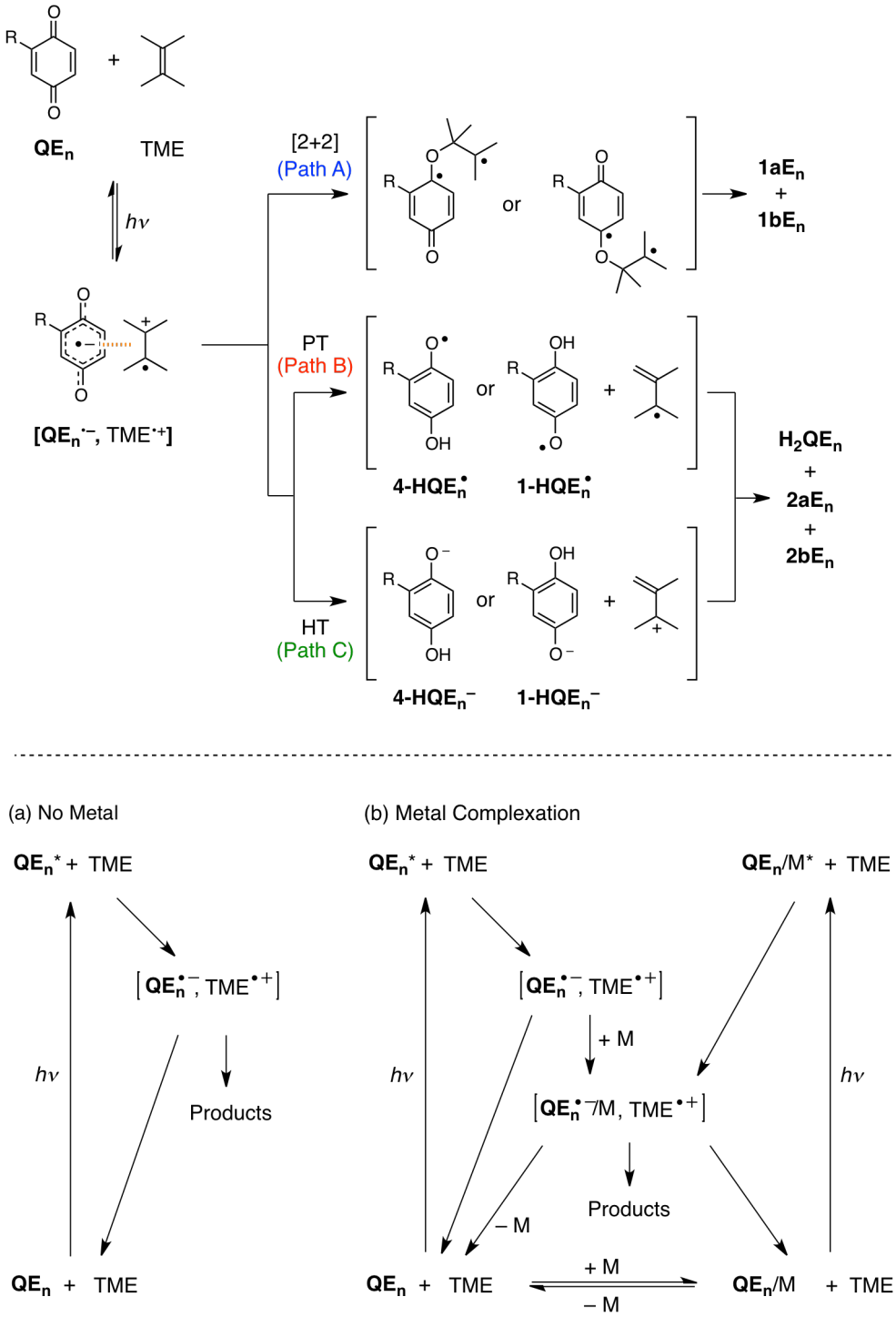

after the HT reaction in path C, proton transfer and ion coupling reactions of the tertiary allyl cation with the hydroquinone anion (4-$\mathbf{HQE_0^-}$ or 1-$\mathbf{HQE_0^-}$) provide the same products. $\mathbf{QE_3}$, having an oligoether sidearm, affords dominantly the PT/HT products (Figure S5b). The

observed difference in ratio of the [2+2] adducts to the PT and HT products in the reactions of **QE$_3$** and **QE$_0$** can be explained by the slightly different electric characters of the attached substituent groups (entry 1 in Table 1, and entry 6 in Table 2).

Photochemical Reactions of Metal Ion Complexes of QE$_n$ with TME.

In the absence of a metal salt, [2+2] cycloaddition and PT/HT reactions equally occur with **QE$_0$**, whereas the PT/HT reaction dominantly occurs with **QE$_3$** (Table 1 and 2). Both the reactions give the hydroquinone as the major product. The product yields and selectivity of the reactions are changed upon addition of alkaline and alkaline earth metal ions into the reaction systems. The photochemical reactions of **QE$_n$** (n = 0 or 3) with TME were performed in MeCN containing 10 equiv. of the metal ion for 20 min. In the case of **QE$_0$**, without an oligoether sidearm, the yield of hydroquinone **H$_2$QE$_0$** was slightly increased with monovalent Na^+, while the yield of **2aE$_0$** increased at the expense of other products in cases with divalent ions Mg^{2+} and Ca^{2+} (entry 6–9 in Table 2, and Figure 3a). The selectivity (%) of the PT/HT products for [2+2] adducts, defined as [(**H$_2$QE$_n$** + **2aE$_n$** + **2bE$_n$** – **1aE$_n$** – **1bE$_n$**)/(**H$_2$QE$_n$** + **2aE$_n$** + **2bE$_n$** + **1aE$_n$** + **1bE$_n$**)] × 100, is increased in the following order; without metal (0%) < Na^+ (18%) < Mg^{2+} (24%) < Ca^{2+} (58%) (Figure 3c, black bars). In the case with Ca^{2+}, the total yield of the PT/HT products (**H$_2$QE$_0$**, **2aE$_0$**, and **2bE$_0$**) was slightly increased from 31% to 42% at the expense of [2+2] adducts (**1aE$_0$** and **1bE$_0$**) from 31% to 11% (entry 6 and 9 in Table 2). Interestingly, this observed trend dramatically stands out in **QE$_3$**, which can bind a metal ion (Figure 3b). Na^+ increased yields of most of the products with relatively high selectivity of **H$_2$QE$_3$**, while Mg^{2+} and Ca^{2+} increased mainly **2aE$_3$** at the expense of [2+2] adducts (entry 1–4 in Table 1, and Figure 3b). In the case with Ca^{2+}, the total yield of PT/HT products increased from 35% to 60%, while oxetanes decreased from 20% to 2%, where the main product was **2aE$_3$** in 42% yield (Figure S5c). The selectivity of the PT/HT products increased in the following order; without metal (27%) < Mg^{2+} (51%) < Na^+ (57%) < Ca^{2+} (94%) (Figure 3c, purple bars). When the resulting sample solution after the reaction of

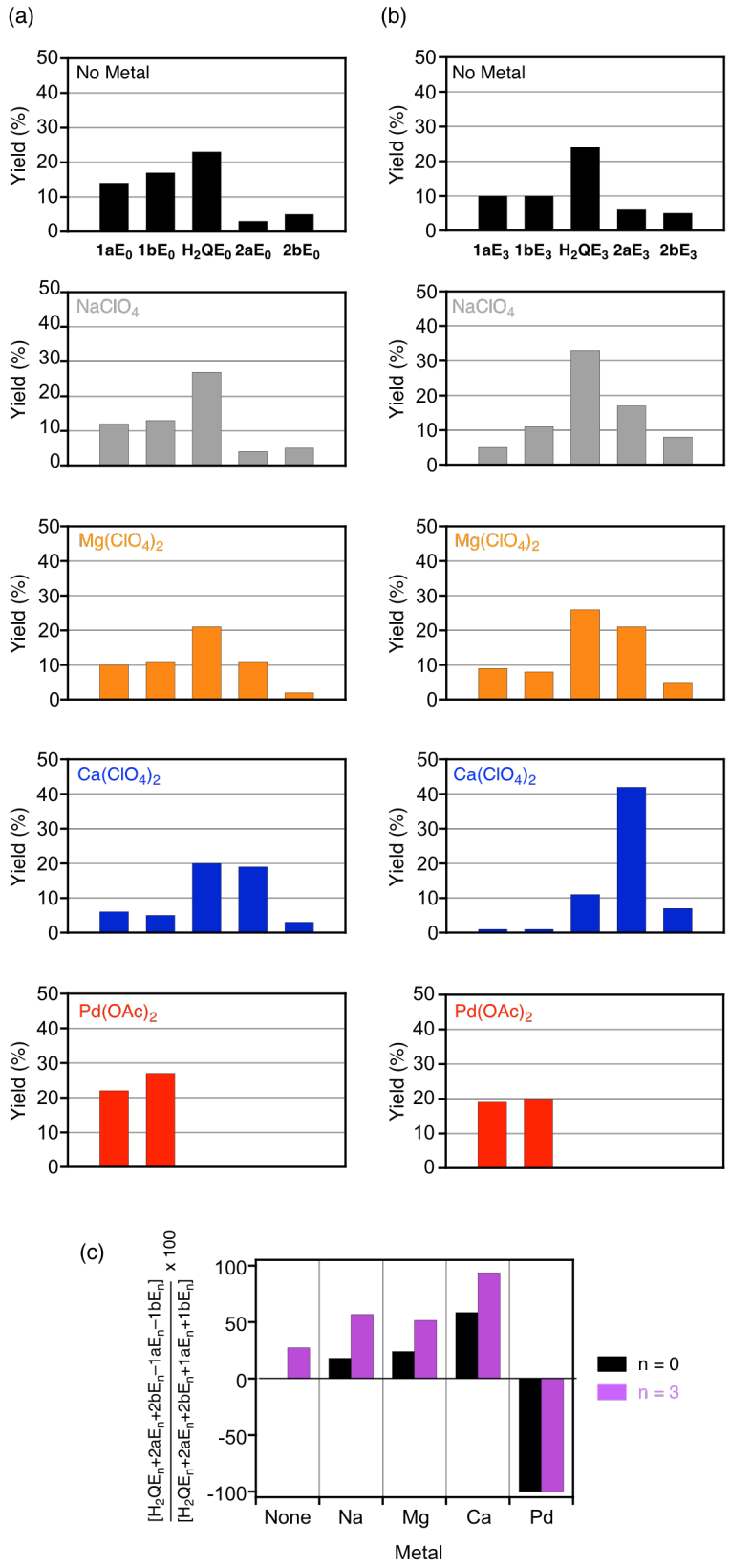

Figure 3. Changes in yields of products when varying added metal salts in the photochemical reaction of $\mathbf{QE_n}$ with TME; (a) n = 0, (b) n = 3. (c) Selectivity (%) of PT/HT products ($\mathbf{H_2QE_n}$, $\mathbf{2aE_n}$, and $\mathbf{2bE_n}$) for [2+2] cycloadducts ($\mathbf{1aE_n}$ and $\mathbf{1bE_n}$).

QE_3 and TME without metal ion (entry 1 in Table 1) was further photoirradiated upon mixing with $Ca(ClO_4)_2$, no notable changes of the product yields were observed. No photoisomerization from oxetane to monoallyl ether adduct occurred upon photoirradiation of the isolated **$1aE_3$** in the presence of Ca^{2+}, either.

Mechanistic Study for the Photochemical Reactions of QE_3/M^{m+} with TME.

The observed trend in the above photochemical reactions of **QE_3** with TME, where yields of the PT/HT products increased at the expense of the oxetanes in the presence of metal ion, indicates that the bound metal ion electronically stabilizes the initial radical ion pair [**$QE_3^{\bullet-}$**, $TME^{\bullet+}$] (Scheme 4b)[19,20] to decelerate the O–C bond formation, when the PT/HT reaction is the major reaction pathway. Here, the oligoether sidearm may assist complexation of the host substrate with the metal ion in the course of photoinduced electron transfer reaction. The proposed electronic interaction in the initial radical ion pair is supported by the fact that metal ions bring about positive shifts of the one-electron reduction potential of **QE_3**, which increases the driving force of electron transfer ($-\Delta G_{ET}$) from TME to ^{3}[**QE_3**$\supset M^{m+}$]* (Table 1). The quantum yields (Φ) of the reactions also increased in the presence of metal ions. Here, the combination of **QE_3** and Ca^{2+}, which forms the most stable divalent complex **QE_3**$\supset Ca^{2+}$, shows the largest change in the one-electron reduction potential, the driving force ($-\Delta G_{ET}$) and the quantum yield. The size-favorable **QE_3**$\supset Ca^{2+}$ complexation may efficiently decelerate the back electron transfer by the electronic interaction between the semiquinone radical anion and the bound metal ion in the radical ion pair [**$QE_3^{\bullet-}$**$\supset Ca^{2+}$, $TME^{\bullet+}$] (Scheme 4b and 5a) (*vide infra*).[20] This electronic interaction withdraws anionic charge of the quinone radical anion with decreasing the charge density, especially at C1 oxygen, but increases the spin density at C4 oxygen. It may subsequently decelerate both the O–C bond formation and the PT reaction in path A and B, respectively, but accelerates the HT reaction in path C.

Scheme 5. Possible Interactions of [$\mathbf{QE_n}^{\bullet-}$, $TME^{\bullet+}$] PET Complex with (a) Ca^{2+} or (b) $Pd(OAc)_2$.

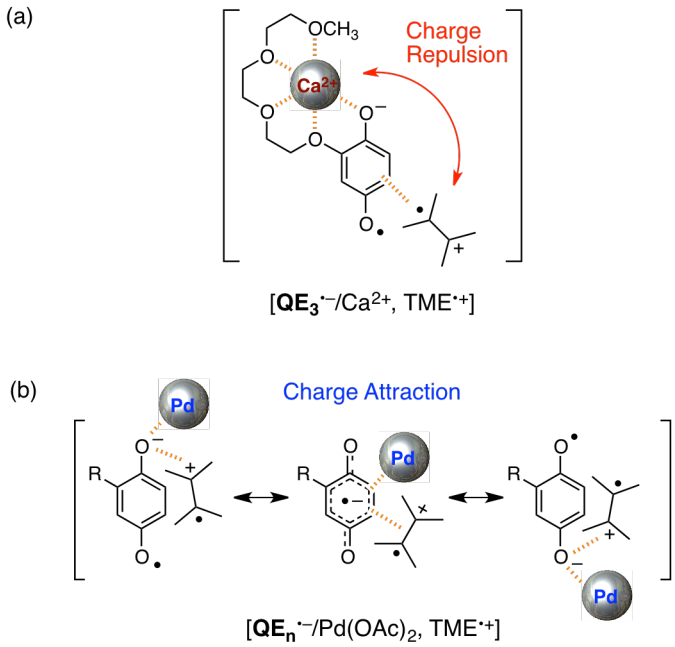

The PT/HT reactions occur at either oxygen of quinone, and the pathway must be highly dependent on the electron and spin densities of the carbonyl groups. We performed DFT calculations at the UB3LYP/6-31+G(d,p) level to evaluate the atomic charge and spin densities of the radical anion of the host quinone $\mathbf{QE_3}^{\bullet-}$ in the absence or presence of $Ca(ClO_4)_2$ (Figure 4, and Supporting Information).[45,46] The results show that the both anionic charge and the spin densities of the quinone oxygens are higher than those of the six-membered ring. Although no notable difference of the charges between the two oxygens of quinone in $\mathbf{QE_3}^{\bullet-}$ is observed without the metal ion, $\mathbf{QE_3}^{\bullet-}\supset Ca^{2+}$ complex shows larger decrease of the anionic charge of $\mathbf{QE_3}^{\bullet-}$, especially at C1 oxygen (from –0.71 to –0.53 at C1 oxygen, from –0.73 to –0.68 at C4 oxygen). The spin density also decreases at C1 oxygen (from 0.26 to 0.21), whereas it increases at C4 oxygen (from 0.22 to 0.25). These results are reasonably explained by the size-favorable complexation, which includes the strong electronic interaction between C1 oxygen and Ca^{2+}. Since both [2+2] and PT reactions (path A and B, respectively) may be decelerated by decreasing the charge density of $\mathbf{QE_3}^{\bullet-}$ upon the

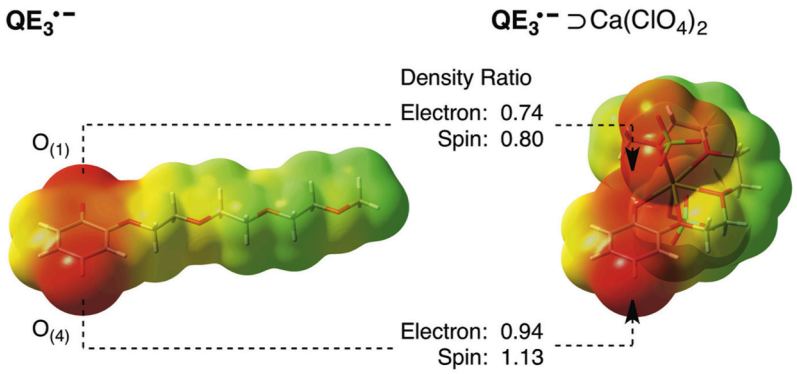

Figure 4. Calculated electron potential maps of (a) $\mathbf{QE_3}^{\bullet-}$ and $\mathbf{QE_3}^{\bullet-}\supset Ca(ClO_4)_2$, with the atomic charge and spin density ratios of $\mathbf{QE_3}^{\bullet-}\supset Ca(ClO_4)_2$ to $\mathbf{QE_3}^{\bullet-}$ on $O_{(1)}$ and $O_{(4)}$ by DFT calculation with UB3LYP/6-31+G(d,p) level.

complexation, the HT reaction (path C) dominantly occurs at C4 oxygen, having the higher spin density, to form an intermediate 4-$\mathbf{HQE_3}^-$. The subsequent bond forming reaction with the allyl cation provides $\mathbf{2aE_3}$. Otherwise, proton transfer from the allyl cation would allow formation of $\mathbf{H_2QE_3}$. The resulting product of 2,3-dimethyl-1,3-butadiene in the reaction mixture was actually detected in the ^{1}H NMR spectroscopic measurements (Figure S10). The unreacted TME and the water included in the solvent may be the candidates of the hydrogen source in the formation of $\mathbf{H_2QE_3}$.

In this mechanism, the observed differences in yields of hydroquinone and its monoallyl ether adducts can also be explained by considering the charge density of hydroquinone anion formed in the possible intermediate metal complex of 4-$\mathbf{HQE_3}^-\supset M^{m+}$. Here, the resulting ionic interaction of 4-$\mathbf{HQE_3}^-$ with the metal ion reduces the charge density of C1 oxygen. This may decelerate the subsequent proton transfer reaction, resulting in the observed increase in $\mathbf{2aE_3}$ formed through the bond forming reaction between 4-$\mathbf{HQE_3}^-$ and the allyl cation.

With these proposed mechanisms, monovalent Na^+, which also forms a size-favorable complex with $\mathbf{QE_3}$ may stabilize the initial radical ion pair of [$\mathbf{QE_3}^{\bullet-}/Na^+$, $TME^{\bullet+}$] (Scheme 4 and 5), but the interaction may be electrically too weak to affect the subsequent reactions,

resulting in increments of the reaction products, except for **1aE$_3$** (Table 1). Actually, the driving force of electron transfer from TME to ^{3}**QE$_3$*** (**–**ΔG_{ET} = 17.8 kcal mol^{-1}) in the presence of Na^+ and the redox potential of **QE$_3$**⊃Na^+ are smaller than those of **QE$_3$**⊃Ca^{2+}.

Photochemical Reactions of Pd(OAc)$_2$-Complexes of QE$_n$ with TME.

In sharp contrast to the cases with alkaline or alkaline earth metal ions, which act as Lewis acids in the photochemical reaction, a transition metal salt of Pd(OAc)$_2$ allowed the selective formation of oxetanes with increases in the product yields (Table 1, 2, and Figure 3). The reactions of **QE$_n$** with TME were carried out in MeCN containing 1.0 equiv. of Pd(OAc)$_2$ for 2.5 h. In comparison with the reactions without or with Pd(OAc)$_2$, the total yields of the oxetanes **1aE$_n$** and **1bE$_n$** increased from 31% to 49% and from 20% to 39% at the expense of all the other products in **QE$_0$** and **QE$_3$**, respectively (entry 10 in Table 2 and entry 5 in Table 1, respectively, and Figure S11). The starting quinone and formation of other products were not observed after the reactions. When the reaction was monitored by ^{1}H NMR spectroscopy, dominant formations of the oxetanes were also observed in the course of reaction (Figure S12 and S13). Furthermore, no isomerization reaction from the monoallyl ether to the oxetane occurred upon photoirradiation of the isolated **2aE$_3$** by mixing with Pd(OAc)$_2$. Therefore, the observed changes in the yields and selectivity of the products can also be explained by the complexations of Pd(OAc)$_2$ with **QE$_n$** and with [**QE$_n$**$^{\bullet-}$, TME$^{\bullet+}$] (Scheme 4b). Since the driving force of electron transfer from TME to ^{3}**QE$_3$*** in the presence of Pd(OAc)$_2$ (–ΔG_{ET} = 7.1 kcal mol^{-1}) is smaller than that without metal ion and Pd(OAc)$_2$ absorbs visible light, the quantum yield of the reaction decreased to 0.06 (entry 5 in Table 1). As discussed in the ^{1}H NMR spectroscopic study described above, Pd(OAc)$_2$ most likely forms a metal–olefin complex with **QE$_3$** in rapid equilibrium in the ground state, where Pd(OAc)$_2$ is electronically neutral. In such a case Pd(OAc)$_2$ may stabilize the semiquinone radical anion in [**QE$_n$**$^{\bullet-}$, TME$^{\bullet+}$], formed through photoinduced electron transfer reaction, by coordination bonding without large separation of **QE$_n$**$^{\bullet-}$ and TME$^{\bullet+}$ to accelerate the O–C bond formation (Scheme

4b, and Scheme 5b).[33]

DFT calculation with UB3PW91/LANL2DZ level of the possible complex of $\mathbf{QE_0}^{\bullet-}$ and $Pd(OAc)_2$, with a hypothesis that $Pd(OAc)_2$ coordinates to C4 oxygen when it catalyze O–C bond formation, shows increase and decrease of the atomic charge and spin density, respectively, at C4 oxygen, and vise versa at C1 oxygen (Figure 5 and Supporting Information).[45,46] $Pd(OAc)_2$ may interact with the anion to allow charge and spin localizations without decreases in their densities, and thus, become a template for O–C bond formation, resulting in selective formation of the oxetanes to increase the yields.[16] Since no notable change of the product ratio of $\mathbf{1aE_n}$ and $\mathbf{1bE_n}$ is observed in the reactions with or without $Pd(OAc)_2$, it can be expected that there is no preference in interactions of $Pd(OAc)_2$ with C1 or C4 oxygen.

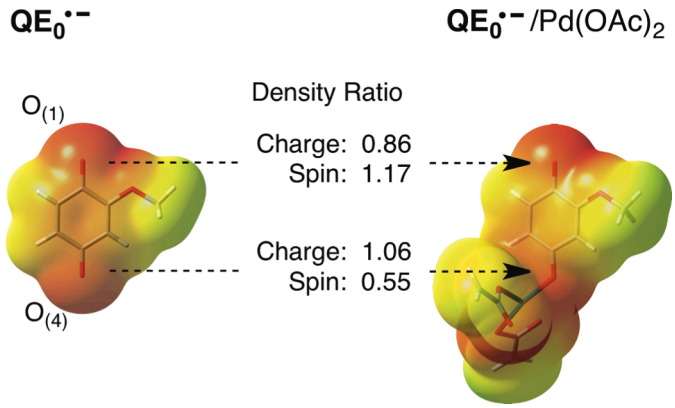

Figure 5. Calculated electron potential maps of $\mathbf{QE_0}^{\bullet-}$ and a possible $\mathbf{QE_0}^{\bullet-}/Pd(OAc)_2$ complex formed through $O_{(4)}$–Pd interaction with the atomic charge and spin density ratios of $\mathbf{QE_0}^{\bullet-}/Pd(OAc)_2$ to $\mathbf{QE_0}^{\bullet-}$ on $O_{(1)}$ and $O_{(4)}$ by DFT calculation with UB3PW91/LANL2DZ level.

Detections of Ca^{2+} and $Pd(OAc)_2$ Complexes of the Semiquinone Radical Anion.

The $\mathbf{QE_3}^{\bullet-}/Ca^{2+}$ and $\mathbf{QE_3}^{\bullet-}/Pd(OAc)_2$ complexes were successfully detected by absorption spectroscopy and ESR in photoinduced electron transfer from dimeric 1-benzyl-1,4-dihydronicotinamide [$(BNA)_2$] to $\mathbf{QE_3}$ in the presence of $Ca(ClO_4)_2$ or $Pd(OAc)_2$, respectively, in MeCN (eq 2).[20,47] The $(BNA)_2$ is known to act as a two-electron donor to

produce the radical anions of electron acceptors.[48]

$$2\mathbf{QE_3} + (BNA)_2 \xrightarrow{h\nu} 2\mathbf{QE_3}^{\bullet-} + 2BNA^{+} \qquad (2)$$

The difference spectrum of the UV/Vis absorption spectra of $\mathbf{QE_3}^{\bullet-}$ and $\mathbf{QE_3}$ provided λ_{max} at 420 nm with a shoulder around 450–550 nm (Figure 6a). The spectral profile dramatically changed in the presence of $Ca(ClO_4)_2$ or $Pd(OAc)_2$ (Figure 6b and 6c, respectively). The absorption bands were red-shifted to 427 nm and 550–800 nm with $Ca(ClO_4)_2$, while a broad absorption band appeared in the range of 400–800 nm with $Pd(OAc)_2$. These different spectra strongly indicate formation of the metal complexes of $\mathbf{QE_3}^{\bullet-}$, generated upon photoirradiation with Ca^{2+} or $Pd(OAc)_2$.

The ESR spectrum of $\mathbf{QE_3}^{\bullet-}$ in the absence of the metal salt was also observed at g = 2.0055 with hyperfine splitting due to three inequivalent protons with a(3H) = 0.98, 2.14, and 3.63 G and two equivalent protons with a(2H) = 0.86 G of $\mathbf{QE_3}^{\bullet-}$ at 243 K in Figure 7a. These hyperfine coupling constants are determined by a computer-simulated spectrum that agrees well with the observed spectrum. Further, these constants are consistent with those predicted by the DFT calculation at the UB3LYP/6-311G(d) level (Figure S14). The ESR spectrum was changed to the spectra at g = 2.0049 with a(3H) = 1.13, 1.80, and 3.66 G, a(2H) = 0.80 G in the presence of $Ca(ClO_4)_2$ at 298 K (Figure 7b), or g = 2.0057 with a(3H) = 2.75, 0.90, and 1.07 G, a(2H) = 1.95 G in the presence of $Pd(OAc)_2$ at 243 K (Figure 7c). These results also indicate that the radical anion of quinone forms metal complexes with Ca^{2+} and $Pd(OAc)_2$, respectively. The smaller or larger g values observed with $Ca(ClO_4)_2$ or $Pd(OAc)_2$, respectively, suggest decrease or increase in the π-electron spin density of the radical anion of quinone when it forms the complex.[49] The results agree well with those revealed by the DFT calculations as shown in Figure 4 and 5. The evaluated hyperfine coupling constants for $\mathbf{QE_3}^{\bullet-}$ /$Pd(OAc)_2$ complex by the DFT calculation at UB3LYP/LANL2DZ level, also suggest that $Pd(OAc)_2$ interacts with the radical anion of quinone mainly through C5–C6 bond of the

quinone (Figure S14). Electrospray Ionization Fourier Transform Mass Spectrometry

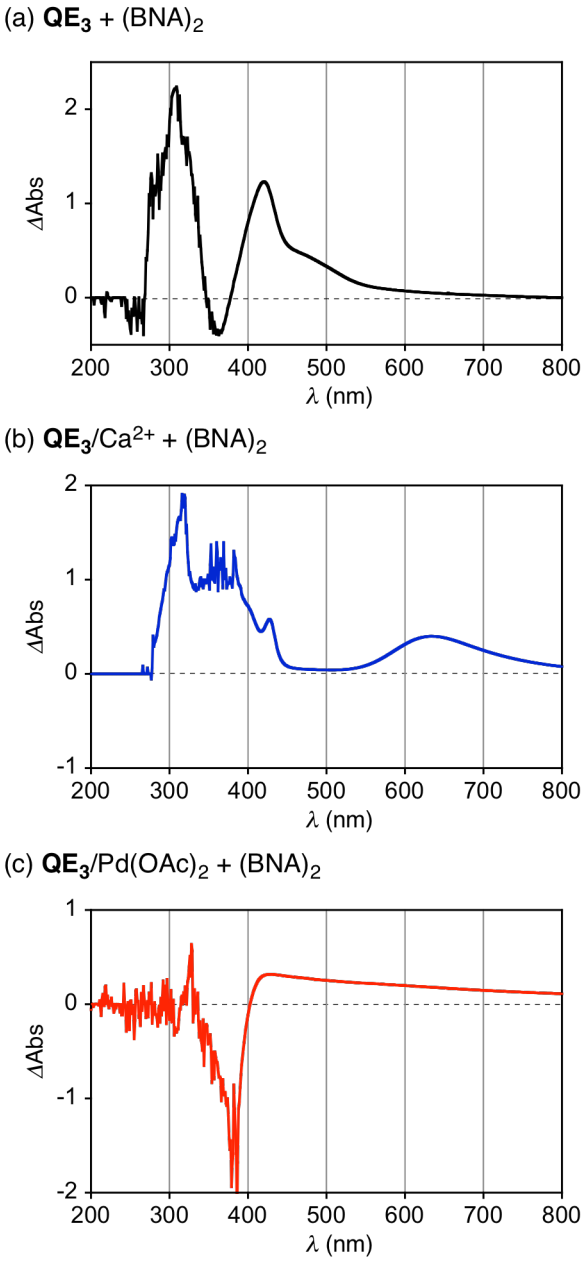

Figure 6. Difference spectra in UV/Vis absorption of (a) $\mathbf{QE_3}$, (b) $\mathbf{QE_3}$/$Ca(ClO_4)_2$, or (c) $\mathbf{QE_3}$/$Pd(OAc)_2$ with $(BNA)_2$ after photoirradiation in deaerated MeCN at 293 K. [$\mathbf{QE_3}$] = 0.33 mM, $Ca(ClO_4)_2$ = 3.3 mM, [$(BNA)_2$] = [$Pd(OAc)_2$] = excess.

(ESI-FT-MS) for the sample solution, containing $\mathbf{QE_3}^{\bullet-}$/$Pd(OAc)_2$ complex, prepared upon photoirradiation of a mixture of $\mathbf{QE_3}$, $Pd(OAc)_2$, and $(BNA)_2$, in the negative ion mode showed a peak at m/z = 495.04 in a complicated mass profile owing to the clusters of

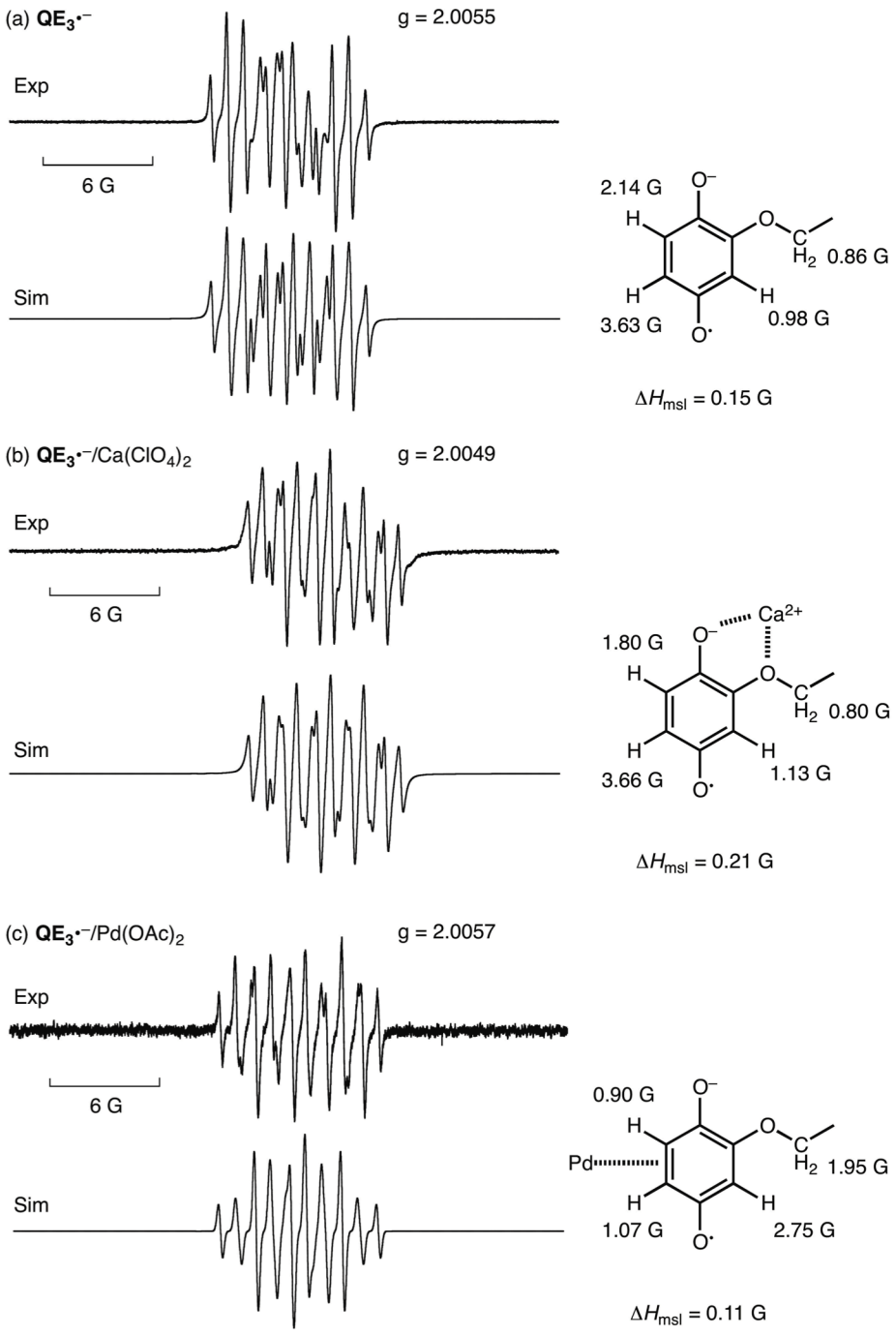

Figure 7. ESR spectra of (a) $\mathbf{QE_3}^{\bullet-}$, (b) $\mathbf{QE_3}^{\bullet-}/Ca(ClO_4)_2$ complex, and (c) $\mathbf{QE_3}^{\bullet-}/Pd(OAc)_2$ complex generated by the photo-irradiation of $\mathbf{QE_3}$ (5.0 mM) with $(BNA)_2$ (excess) in the absence or presence of 50.0 mM $Ca(ClO_4)_2$ or 5.0 mM $Pd(OAc)_2$ in deaerated MeCN with the computer simulation spectra, the hyperfine coupling constants, and the maximum slope line widths (ΔH_{msl}). The spectral measurements of (a) and (c), and (b) were demonstrated at 243 K and 298 K, respectively.

$Pd(OAc)_2$, which corresponds to its hydrogenated form with the calculated mass of 495.05 (Figure S15). The observed isotope pattern is almost consistent with the calculated one.

[$\mathbf{QE_3}^{\bullet-}$, $TME^{\bullet+}$] as an intermediate of photoinduced electron transfer was also detected by ESR in a MeCN solution, containing a 1:4 mixture of $\mathbf{QE_3}$ and TME under exposure to light at 77 K. The ESR spectrum in the absence of the metal salt was observed at g = 2.0050 without hyperfine splitting (Figure S16). The g value was shifted to 2.0048 or 2.0054 in the presence of 10 equiv. $Ca(ClO_4)_2$ or 1.0 equiv. $Pd(OAc)_2$, respectively. Since the observed shifts of g values in the presence of Ca^{2+} and $Pd(OAc)_2$ agree with those observed in $\mathbf{QE_3}^{\bullet-}/Ca^{2+}$ and $\mathbf{QE_3}^{\bullet-}/Pd(OAc)_2$ complexes generated by $(BNA)_2$, [$\mathbf{QE_3}^{\bullet-}$, $TME^{\bullet+}$] complex most likely forms the ternary complexes with Ca^{2+} or $Pd(OAc)_2$.

Conclusion

Photochemical reactions of $\mathbf{QE_n}$ (n = 0 and 3) with TME, which proceed through the photoinduced electron transfer mechanism, provide multi photoproducts of oxetanes $\mathbf{1aE_n}$ and $\mathbf{1bE_n}$, and hydroquinone $\mathbf{H_2QE_n}$ as major products, and monoallyl ether adducts of hydroquinone $\mathbf{2aE_n}$ and $\mathbf{2bE_n}$. $\mathbf{QE_3}$, having a long oligoether sidearm, selectively provides $\mathbf{2aE_3}$ when it forms a size-favorable host–guest complex with Ca^{2+}. The oxetanes are selectively produced when $\mathbf{QE_n}$ forms metal–olefin complexes with $Pd(OAc)_2$. ^1H NMR spectroscopy revealed that $\mathbf{QE_3}$ binds Ca^{2+} and $Pd(OAc)_2$ through electrostatic interaction and metal–olefin interaction, respectively. Cyclic voltammetry also showed that Ca^{2+} strongly withdraws electrons from the quinone moiety, whereas $Pd(OAc)_2$ has no electronic effect on the quinone reduction. DFT calculations also indicated that such metal complexations of $\mathbf{QE_n}$ resulted in changing electronic structures of the intermediate semiquinone radical anion $\mathbf{QE_n}^{\bullet-}$. Ca^{2+} strongly withdraws electrons from the quinone through C1 oxygen in both $\mathbf{QE_3}\supset Ca^{2+}$ complex and the [$\mathbf{QE_3}^{\bullet-}\supset Ca^{2+}$, $TME^{\bullet+}$] photoinduced electron transfer complex to reduce the electron density of the quinone. $Pd(OAc)_2$ allows localization of the anionic charge around the coordination bond with $Pd(OAc)_2$ in [$\mathbf{QE_n}^{\bullet-}/Pd(OAc)_2$, $TME^{\bullet+}$] complex without decrease of

the charge density of the quinone radical anion. The Ca^{2+} and $Pd(OAc)_2$ complexes of $\mathbf{QE_3}^{\bullet-}$ have been successfully characterized in the absorption and ESR spectroscopy. The ternary complex [$\mathbf{QE_3}^{\bullet-}$/metal, $TME^{\bullet+}$] formed upon photoirradiation, thus, determines the favorable reaction pathway of the [2+2] cycloaddition, PT and HT reactions. The present supramolecular photochemical reactions suggest their importance for the design of the electronic interactions of reaction substrates and the intermediate radical ion pair with the catalyst in controlling a variety of photochemical reaction pathways that proceed by the photoinduced electron transfer mechanism.

Experimental Section

Materials. Unless otherwise noted, reagents and solvents were used as received from Tokyo Kasei Co., Ltd. (TCI) [methoxy-*p*-benzoquinone $\mathbf{QE_0}$ (>99%) and tetramethylethylene TME (>96%)], Wako Pure Chemical Industries, Ltd. [sodium perchlorate (>95%), acetonitrile (>99.5) and acetonitrile-d_3 (>99.8%)], Sigma Aldrich [calcium perchlorate tetrahydrate (>99%) and magnesium perchlorate], and Kishida Chemical Co., Ltd. [chloroform (>99%) and hexane (>95%)]. $\mathbf{QE_3}$ was prepared as described in our previous report. All products were unambiguously characterized by means of ^{1}H and ^{13}C NMR, and IR spectroscopies, and Electrospray Ionization Fourier Transform Mass Spectrometry. Oxetanes $\mathbf{1aE_n}$ and $\mathbf{1bE_n}$, and monoallyl ether adducts of hydroquinone $\mathbf{2aE_n}$ and $\mathbf{2bE_n}$ were also characterized by reference to ref. 29d and ref. 31, respectively.

Measurements. ^{1}H and ^{13}C NMR spectra were recorded on a Varian INOVA 400 spectrometer (400 MHz for ^{1}H and 100 MHz for ^{13}C) or a Bruker AVANCE 500 spectrometer (500 MHz for ^{1}H and 125 MHz for ^{13}C). Chemical shifts (δ in ppm) were reported with respect to tetramethylsilane as the internal standard. Infrared absorption spectra (IR) were recorded on a JASCO FT/IR-4200 Fourier transform infrared spectrometer. Electronic absorption spectra were recorded using a Hewlett-Packard HP8453 diode array spectrophotometer. Phosphorescence spectra were recorded using a JASCO FP-6600 fluorescence spectrometer. Elemental analyses were performed on a YANACO CHN Corder MT-5. Fourier transform mass spectrometry was performed on a Thermo Fisher Scientific LTQ Orbitrap Discovery. Analytical HPLC were performed at 20 °C on a COSMOSIL 5C_{18}-MS-II column (ø4.6 mm × 250 mm) using a JASCO PU-2080 HPLC pump, equipped with UV-2015 multi-wavelength UV-Vis detector, with MeOH:H_2O (100:0, 80:20, or 65:35) as an eluent.

Cyclic Voltammetry. Electrochemical measurements were made with an ALS 1210A electrochemical analyzer using a glassy carbon working electrode, a platinum wire counter electrode, and an Ag/Ag^+ [0.01 M $AgNO_3$, 0.1 M Bu_4NClO_4 (MeCN)] reference electrode. Scan rate was 100–20 mV s^{-1}. The CV curves were calibrated using the ferrocene/ferrocenium

(Fc/Fc^+) redox couple as an external standard, which was measured under same conditions before and after the measurements of samples. The half-wave potential of Fc/Fc^+ was found to be 0.09 V related to the Ag/Ag^+ reference electrode.

Theoretical Calculations. For calculation of structures and electron potential maps of $\mathbf{QE_3}^{\bullet-}$ and $\mathbf{QE_3}^{\bullet-}\supset Ca(ClO_4)_2$, and $\mathbf{QE_0}^{\bullet-}$ and $\mathbf{QE_0}^{\bullet-}/Pd(OAc)_2$, the density functional theory (UB3LYP/6-31+G(d,p) and UB3PW91/LANL2DZ, respectively) was employed as implemented in the Gaussian 09 set of programs.[45] Stationary structures were identified as those structures where all of the harmonic frequencies were real.

ESR Measurements. The ESR spectra were recorded on a JEOL X-band ESR spectrometer (JES-RE1XE). A quartz ESR tube (internal diameter: 1.8 mm and 4.5 mm) containing a sample at 298, 243, or 77 K was irradiated in the cavity of the ESR spectrometer with the focused light of a 1000 W high-pressure Hg lamp (Ushio-USH1005D) through an aqueous filter. The ESR spectra were measured under nonsaturating microwave power conditions. The amplitude of modulation was chosen to optimize the resolution and the signal-to-noise (S/N) ratio of the observed spectra. The *g* values were calibrated with a Mn^{2+} marker. Simulations of ESR signals were made by using a WinSIM program.[50]

A Typical Procedure for Photochemical Reactions of $\mathbf{QE_n}$ (n = 0 and 3). To an acetonitrile solution (0.5 mL) of $\mathbf{QE_n}$ (5×10^{-3} mmol) was added 4 equiv. TME (20×10^{-3} mmol) with or without 10 equiv. metal perchlorate (Na^+, Mg^{2+}, or Ca^{2+}) or 1 equiv. $Pd(OAc)_2$ in a Pyrex glass tube and the mixture solution was degased by argon bubbling for 5 min. The solution was irradiated by 500 W xenon lamp (USHIO SPAX INC., SX-UID502XAM) equipped with a >420 nm optical filter (Kansai Chemical Engineering Co. Ltd., GG420). The reactions were demonstrated for 20 min in the cases with or without the metal perchlorate, and for 150 min in the case with $Pd(OAc)_2$. The sample solution was then analyzed by HPLC, equipped with COSMOSIL $5C_{18}$-MS-II column (ø4.6 mm × 250 mm), with MeOH:H_2O (100:0, 80:20, or 65:35) as an eluent.

Isolations of $\mathbf{H_2QE_n}$, $\mathbf{2aE_n}$, and $\mathbf{2bE_n}$ (n = 0 and 3). To an acetonitrile solution (6 mL) of

QE_n (1.45 mmol) was added 4 equiv. TME (5.80 mmol) in a Pyrex glass tube, and the mixture solution was degased by argon bubbling for 10 min. The solution was irradiated by 500 W xenon lamp (USHIO SPAX INC., SX-UID502XAM) equipped with a >420 nm optical filter (Kansai Chemical Engineering Co. Ltd., GG420) for 3 h. The sample solution was then evaporated to dryness. The brown oil was obtained, and the residue was separated through preparative HPLC, equipped with COSMOSIL $5C_{18}$-MS-II column (ø10.0 mm × 250 mm), with MeOH:H_2O (80:20) as an eluent.

Isolations of $1aE_n$ and $1bE_n$ (n = 0 and 3). To an acetonitrile solution (5 mL) of **QE_n** (0.036 mmol) was added 8 equiv. TME (0.288 mmol) and 1 equiv. $Pd(OAc)_2$ (0.036 mmol) in a Pyrex glass tube and the mixture solution was degased by argon bubbling for 10 min. The solution was irradiated by 500 W xenon lamp (USHIO SPAX INC., SX-UID502XAM) equipped with a >420 nm optical filter (Kansai Chemical Engineering Co. Ltd., GG420) for 4 h. The sample solution was then evaporated to dryness. The brown oil was obtained and the residue was separated through flash silica gel column chromatography with hexane:chloroform (30:70) and hexane:ethyl acetate (20:80) as an eluent for **$1aE_0$** and **$1bE_0$**, and **$1aE_3$** and **$1bE_3$**, respectively.

5-Methoxy-2,2,3,3-tetramethyl-1-oxaspiro[3.5]nona-5,8-dien-7-one ($1aE_0$): ^{1}H NMR (500 MHz, $CDCl_3$, 20 °C): δ 7.06 (d, 1H, J = 10.1 Hz), 6.05 (dd, 1H, J = 10.1, 2.0 Hz), 5.45 (d, 1H, J = 1.9 Hz), 3.83 (s, 3H), 1.50 (s, 6H), 1.17 (s, 3H), 1.13 (s, 3H); ^{13}C NMR (125 MHz, $CDCl_3$, 20 °C): δ 187.1, 174.5, 147.7, 126.8, 102.0, 86.7, 82.8, 55.4, 50.7, 27.2, 25.2, 22.3, 20.9; IR (KBr): 3449, 2965, 1657, 1588, 1459, 1360, 1227, 1165, 1096, 1059, 980, 851 cm^{-1}; Anal. Calcd for $C_{13}H_{18}O_3$: C, 70.24; H, 8.16. Found: C, 68.32; H, 8.59; HRMS (ESI): m/z calcd for ($C_{13}H_{18}O_3 + H^+$) 223.1334, found 223.1327.

6-Methoxy-2,2,3,3-tetramethyl-1-oxaspiro[3.5]nona-5,8-dien-7-one ($1bE_0$): ^{1}H NMR (500 MHz, $CDCl_3$, 20 °C): δ 7.29 (dd, 1H, J = 10.9, 2.9 Hz), 6.15 (d, 1H, J = 10.9 Hz), 6.06 (d, 1H, J = 2.8 Hz), 3.72 (s, 3H), 1.51 (s, 3H), 1.48 (s, 3H), 1.23 (s, 3H), 1.17 (s, 3H); ^{13}C NMR (125 MHz, $CDCl_3$, 20 °C): δ 180.4, 150.9, 149.9, 127.1, 116.0, 85.6, 81.7, 55.0, 49.2, 27.1, 27.0, 22.6, 21.8; IR (KBr): 2924, 2360, 2341, 1674, 1638, 1609, 1455, 1369, 1209, 1106, 935, 882,

629 cm^{-1} ; HRMS (ESI): m/z calcd for ($C_{13}H_{18}O_3$ + H^+) 223.1334, found 223.1332.

3-Methoxy-4-[(1,1,2-trimethyl-2-propene-1-yl)oxy]-phenol (2aE_0): ^{1}H NMR (500 MHz, $CDCl_3$, 20 °C): δ 6.80 (d, 1H, J = 8.7 Hz), 6.41 (d, 1H, J = 2.9 Hz), 6.23 (dd, 1H, J = 8.7, 2.8 Hz), 5.05 (s, 1H, -OH), 4.94 (s, 1H), 4.90 (s, 1H), 3.75 (s, 3H), 1.93 (s, 3H), 1.41 (s, 6H); ^{13}C NMR (125 MHz, $CDCl_3$, 20 °C): δ 153.4, 151.3, 150.3, 138.8, 122.2, 111.1, 105.9, 100.5, 81.9, 55.7, 26.0, 19.0; IR (KBr): 3343, 2988, 2965, 1603, 1510, 1452, 1382, 1366, 1347, 1298, 1203, 1163, 1110, 1037, 957, 907, 850, 832, 815, 663 cm^{-1}; Anal. Calcd for $C_{13}H_{18}O_3$: C, 70.24; H, 8.16; Found: C, 69.39; H, 8.30. HRMS (ESI): m/z calcd for ($C_{13}H_{18}O_3$ + H^+) 223.1334, found 223.1330.

2-Methoxy-4-[(1,1,2-trimethyl-2-propene-1-yl)oxy]-phenol (2bE_0): ^{1}H NMR (500 MHz, $CDCl_3$, 20 °C): δ 6.73 (d, 1H, J = 8.5 Hz), 6.53 (d, 1H, J = 2.5 Hz), 6.48 (dd, 1H, J = 8.7, 2.5 Hz), 5.25 (s, 1H, -OH), 4.96 (s, 1H), 4.93 (s, 1H), 3.82 (s, 3H), 1.90 (s, 3H), 1.44 (s, 6H); ^{13}C NMR (125 MHz, $CDCl_3$, 20 °C): δ 150.6, 149.6, 146.3, 140.4, 113.6, 112.1, 111.1, 104.6, 88.8, 55.8, 26.7, 18.9; IR (KBr): 3423, 2982, 1609, 1509, 1450, 1376, 1263, 1230, 1198, 1156, 1135, 1037, 965 cm^{-1}; HRMS (ESI): m/z calcd for ($C_{13}H_{18}O_3$ + H^+) 223.1332, found 223.1330.

5-(2'-(2''-(2'''-Methoxyethoxy)ethoxy)ethoxy)-2,2,3,3-tetramethyl-1-oxaspiro[3.5]nona-5,8-dien-7-one (1aE_3): ^{1}H NMR (500 MHz, $CDCl_3$, 20 °C): δ 7.04 (d, 1H, J = 10.2 Hz), 6.05 (dd, 1H, J = 10.2, 1.6 Hz), 5.41 (d, 1H, J = 1.6 Hz), 4.10–3.54 (m, 12H), 3.38 (s, 3H), 1.51 (s, 3H), 1.48 (s, 3H), 1.20 (s, 3H) , 1.13 (s, 3H); ^{13}C NMR (125 MHz, $CDCl_3$, 20 °C): δ 187.1, 173.7, 147.7, 126.9, 102.4, 86.8, 82.7, 72.0, 70.8, 70.7, 70.6, 68.8, 67.7, 59.1, 50.8, 27.4, 25.0, 22.5, 20.9; IR (KBr): 3504, 2926, 1656, 1623, 1585, 1415, 1374, 1349, 1226, 1097, 1057, 983, 946, 851, 803 cm^{-1}; Anal. Calcd for $C_{19}H_{30}O_6$: C, 64.38; H, 8.53. Found: C, 64.45; H, 8.24; HRMS (ESI): m/z calcd for ($C_{19}H_{30}O_6$ + H^+) 355.2121, found 355.2111.

6-(2'-(2''-(2'''-Methoxyethoxy)ethoxy)ethoxy)-2,2,3,3-tetramethyl-1-oxaspiro[3.5]nona-5,8-dien-7-one (1bE_3): ^{1}H NMR (500 MHz, $CDCl_3$, 20 °C): δ 7.26 (dd, 1H, J = 10.1, 2.9 Hz), 6.13 (d, 1H, J = 10.1 Hz), 6.11 (d, 1H, J = 2.8 Hz), 4.00–3.98 (m, 2H), 3.88–3.85 (m, 2H), 3.74–3.72 (m, 2H), 3.68–3.63 (m, 4H), 3.57–3.55 (m, 2H), 3.38 (s, 3H), 1.50 (s, 3H), 1.47 (s, 3H), 1.21 (s, 3H), 1.16 (s, 3H); ^{13}C NMR (125 MHz, $CDCl_3$, 20 °C): δ 181.1, 150.5, 149.2, 127.2, 117.3, 85.5, 81.7, 71.9, 70.9, 70.6, 70.5, 69.0, 67.3, 59.0, 49.3, 27.0, 26.9, 22.5, 21.8;

IR (KBr): 2921, 1675, 1637, 1608, 1457, 1375, 1272, 1236, 1194, 1091, 1020, 876, 630, 524, 504 cm^{-1}; HRMS (ESI): m/z calcd for ($C_{19}H_{30}O_6 + H^+$) 355.2121, found 355.2117.

2-(2'-(2''-(2'''-Methoxyethoxy)ethoxy)ethoxy)-hydroquinone (H_2QE_3): ^1H NMR (500 MHz, $CDCl_3$, 20 °C): δ 6.74 (d, 1H, J = 8.5 Hz), 6.49 (d, 1H, J = 2.9 Hz), 6.37 (dd, 1H, J = 8.5, 2.9 Hz), 4.09–4.07 (m, 2H), 3.79–3.78 (m, 2H), 3.71–3.58 (m, 6H), 3.58–3.56 (m, 2H), 3.38 (s, 3H); ^{13}C NMR (125 MHz, $CDCl_3$, 20 °C): δ 149.4, 146.3, 140.6, 115.4, 108.5, 103.0, 71.9, 70.5, 70.4, 70.3, 69.6, 69.2, 58.9; IR (KBr): 3269, 2898, 1616, 1515, 1457, 1351, 1293, 1201, 1171, 1110, 986, 840, 801 cm^{-1}; HRMS (ESI): m/z calcd for ($C_{13}H_{20}O_6 + H^+$) 273.1338, found 273.1335.

3-(2'-(2''-(2'''-Methoxyethoxy)ethoxy)ethoxy)-4-[(1,1,2-trimethyl-2-propene-1-yl)oxy]-phenol ($2aE_3$): ^1H NMR (500 MHz, $CDCl_3$, 20 °C): δ 6.79 (d, 1H, J = 8.6 Hz), 6.57 (d, 1H, J = 2.8 Hz), 6.30 (dd, 1H, J = 8.6, 2.8 Hz), 6.06 (s, 1H, -OH), 4.95 (s, 1H), 4.89 (s, 1H), 4.10–4.08 (m, 2H), 3.77–3.75 (m, 2H), 3.72–3.70 (m, 2H), 3.68–3.65 (m, 4H), 3.63–3.60 (m, 2H), 3.41 (s, 3H), 1.93 (s, 3H), 1.39 (s, 6H); ^{13}C NMR (125 MHz, $CDCl_3$, 20 °C): δ 152.5, 151.9, 150.3, 139.3, 123.2, 110.9, 107.4, 104.3, 81.9, 72.0, 70.6, 70.2, 69.6, 68.9, 58.9, 25.9, 19.0; IR (KBr): 3366, 2981, 2921, 1646, 1599, 1508, 1455, 1376, 1361, 1298, 1216, 1176, 1132, 990, 933, 909, 862 cm^{-1}; HRMS (ESI): m/z calcd for ($C_{19}H_{30}O_6 + H^+$) 355.2121, found 355.2111.

2-(2'-(2''-(2'''-Methoxyethoxy)ethoxy)ethoxy)-4-[(1,1,2-trimethyl-2-propene-1-yl)oxy]-phenol ($2bE_3$): ^1H NMR (500 MHz, $CDCl_3$, 20 °C): δ 6.74 (d, 1H, J = 8.8 Hz), 6.56 (d, 1H, J = 2.9 Hz), 6.52 (dd, 1H, J = 8.8, 2.6 Hz), 6.36 (s, 1H, -OH), 4.95 (s, 1H), 4.91 (s, 1H), 4.11–4.09 (m, 2H), 3.81–3.79 (m, 2H), 3.73–3.72 (m, 2H), 3.70–3.68 (m, 2H), 3.67–3.65 (m, 2H), 3.57–3.55 (m, 2H), 3.38 (s, 3H), 1.89 (s, 3H), 1.42 (s, 6H); ^{13}C NMR (125 MHz, $CDCl_3$, 20 °C): δ 150.5, 149.2, 145.6, 142.3, 114.7, 114.3, 111.1, 108.5, 80.8, 71.9, 70.7, 70.6, 70.5, 69.7, 69.5, 59.0, 26.7, 18.9; IR (KBr): 3434, 2981, 2925, 1646, 1604, 1509, 1455, 1376, 1234, 1200, 1170, 1132, 989, 902, 857 cm^{-1}; HRMS (ESI): m/z calcd for ($C_{19}H_{30}O_6 + H^+$) 355.2121, found 355.2121.

Acknowledgements

The present work was sponsored by a Grant-in-Aid for Scientific Research (B) (No. 25286017) and a Challenging Exploratory Research (No.24655125) from the Ministry of Education, Science, Sports, and Culture, Japan, and a Toray Science and Technology Grant.

Supporting Information

Electronic Supplementary Information (ESI) available: [^{1}H and ^{13}C NMR spectroscopies, and HPLC analyses, X-ray crystallography, mass spectrometry, ESR spectroscopies, and further details on computational calculations.] See DOI: 10.1039/b000000x/

References

(1) D. G. Amirsakis, M. A. Garcia-Garibay, S. J. Rowan, J. F. Stoddart, A. J. P. White and D. J. Williams, *Angew. Chem., Int. Ed.*, 2001, **40**, 4256.

(2) L. Kaanumalle, J. Nithyanandhan, M. Pattabiraman, J. Narayanaswamy and V. Ramamurthy, *J. Am. Chem. Soc.*, 2004, **126**, 8999; L. S. Kaanumalle, R. Ramesh, V. S. N. Murthy Maddipatla, J. Nithyanandhan, N. Jayaraman and V. Ramamurthy, *J. Org. Chem.*, 2005, **70**, 5062.

(3) G. Ananchenko, K. Udachin, J. Ripmeester, T. Perrier and A. Coleman, *Chem.–Eur. J.*, 2006, **12**, 2441.

(4) K. Vízvárdi, K. Desmet, I. Luyten, P. Sandra, G. Hoornaert and E. Van der Eycken, *Org. Lett.*, 2001, **3**, 1173.

(5) Y. Inoue, F. Dong, K. Yamamoto, L.-H. Tong, H. Tsuneishi, T. Hakushi and A. Tai, *J. Am. Chem. Soc.*, 1995, **117**, 11033; Y. Inoue, T. Wada, N. Sugahara, K. Yamamoto, K. Kimura, L. H. Tong, X. M. Gao, Z. J. Hou and Y. Liu, *J. Org. Chem.*, 2000, **65**, 8041; C. Yang, A. Nakamura, T. Wada and Y. Inoue, *Org. Lett.*, 2006, **8**, 3005; C. Yang, T. Mori, Y. Origane, Y. H. Ko, N. Selvapalam, K. Kim and Y. Inoue, *J. Am. Chem. Soc.*, 2008, **130**, 8574.

(6) W. Herrmann, S. Wehrle, G. Wenz, *Chem. Commun.*, 1997, 1709; H. Ikeda, T. Nihei and A. Ueno, *J. Org. Chem.*, 2005, **70**, 1237.

(7) Y. Ishida, Y. Kai, S. Y. Kato, A. Misawa, S. Amano, Y. Matsuoka and K. Saigo, *Angew. Chem., Int. Ed.*, 2008, **47**, 8241.

(8) M. Yoshizawa, Y. Takeyama, T. Kusukawa and M. Fujita, *Angew. Chem., Int. Ed.*, 2002, **41**, 1347; M. Yoshizawa, Y. Takeyama, T. Okano and M. Fujita, *J. Am. Chem. Soc.*, 2003, **125**, 3243; M. Yoshizawa, S. Miyagi, M. Kawano, K. Ishiguro and M. Fujita, *J.*

Am. Chem. Soc., 2004, **126**, 9172; T. Furusawa, M. Kawano and M. Fujita, *Angew. Chem., Int. Ed.* 2007, **46**, 5717; T. Murase, S. Horiuchi and M. Fujita, *J. Am. Chem. Soc.*, 2010, **132**, 2866.

(9) S. Y. Jon, Y. H. Ko, S. H. Park, H.-J. Kim and K. Kim, *Chem. Commun.*, 2001, 1938; R. Wang, L. Yuan and D. H. Macartney, *J. Org. Chem.*, 2006, **71**, 1237.

(10) L. S. Kaanumalle and V. Ramamurthy, *Chem. Commun.*, 2007, 1062.

(11) K. Fujimoto, S. Matsuda, N. Takahashi and I. Saito, *J. Am. Chem. Soc.,* 2000, **122**, 5646; K. Fujimoto, H. Yoshino, T. Ami, Y. Yoshimura and I. Saito, *Org. Lett.*, 2008, **10**, 397.

(12) G. Agati and A. F. McDonagh, *J. Am. Chem. Soc.*, 1995, **117**, 4425; T. Wada, N. Sugahara, M. Kawano and Y. Inoue, *Chem. Lett.*, 2000, 1174.

(13) V. Ramamurthy, J. Shailaja, L. S. Kaanumalle, R. B. Sunoj and J. Chandrasekhar, *Chem. Commun.*, 2003, 1987; H. Garcia and H. D. Roth, *Chem. Rev.*, 2002, **102**, 3947.

(14) T. Bach and H. Bergmann, *J. Am. Chem. Soc.*, 2000, **122**, 11525.

(15) N. D. McClenaghan, C. Absalon and D. M. Bassani, *J. Am. Chem. Soc.*, 2003, **125**, 13004.

(16) J. T. M. Evers and A. Mackor, *Tetrahedron Lett.*, 1978, 821; K. Langer and J. Mattay, *J. Org. Chem.*, 1995, **60**, 7256; Y. V. Pol, R. Suau, E. Perez-Inestrosa and D. Bassani, *Chem. Commun.*, **2004**, 1270.

(17) N. J. Turro, *Proc. Natl. Acad. Sci. U.S.A.*, 2002, **99**, 4805.

(18) C. J. Pedersen, *J. Am. Chem. Soc.*, 1967, **89**, 2495; C. J. Pedersen, *J. Am. Chem. Soc.*, 1967, **89**, 7017; C. J. Pedersen and H. K. Frensdorff, *Angew. Chem., Int. Ed. Engl.,* 1972, **11**, 16.

(19) S. Fukuzumi, T. Okamoto and T. Otera, *J. Am. Chem. Soc.*, 1994, **116**, 5503.

(20) S. Fukuzumi, N. Nishizawa and T. Tanaka, *J. Chem. Soc., Perkin Trans. 2*, 1985, 371; S. Fukuzumi, Y. Fujii and T. Suenobu, *J. Am. Chem. Soc*., 2001, **123**, 10191; K. Okamoto, K. Ohkubo, K. M. Kadish and S. Fukuzumi, *J. Phys. Chem. A*, 2004, **108**, 10405; S. Fukuzumi, K. Ohkubo, J. Ortiz, A. M. Gutiérrez, F. Fernández-Lázaro and Á. Sastre-Santos, *J. Phys. Chem. A*, 2008, **112**, 10744; S. Fukuzumi and K. Ohkubo, *Coord. Chem. Rev*., 2010, **254**, 372.

(21) S. M. Hubig, D. Sun and J. K. Kochi, *J. Chem. Soc., Perkin Trans. 2*, 1999, 781.

(22) H. Wu, D. Zhang, L. Su, K. Ohkubo, C. Zhang, S. Yin, L. Mao, Z. Shuai, S. Fukuzumi and D. Zhu, *J. Am. Chem. Soc*., 2007, **129**, 6839.

(23) A. Tsuda and T. Oshima, *J. Org. Chem.,* 2002, **67**, 1282; A. Tsuda, C. Fukumoto and T. Oshima, *J. Am. Chem. Soc*., 2003, **125**, 5811; K. Kawakami, Y. Sei, K. Yamaguchi and A. Tsuda, *J. Org. Chem*., 2011, **76**, 875.

(24) G. Ercolani and L. Mandlini, *J. Am. Chem. Soc*., 1990, **112**, 423; R. Cacciapaglia and L. Mandlini, *Chem. Soc. Rev*., 1993, 221.

(25) T. Lu, H. K. Yoo, H. Zhang, S. Bott, J. L. Atwood, L. Echegoyen and G. W. Gokel, *J. Org. Chem.,* 1990, **55**, 2269; Y. Naruta, F. Tani, N. Ishihara and K. Maruyama, *J. Am. Chem. Soc*., 1991, **113**, 6865; J. T. Groves and P. Viski, *J. Am. Chem. Soc*., 1989, **111**, 8537; C. Monnereau, P. H. Ramos, A. B. C. Deutman, J. A. A. W. Elemans, R. J. M. Nolte and A. E. Rowan, *J. Am. Chem. Soc*., 2010, **132**, 1529; M. R. Doyle, *Angew. Chem. Int. Ed*., 2009, **48**, 850.

(26) J. Kang and J. Rebek, Jr *Nature*, 1997, **385**, 50; J. L. Hou, D. Ajami and J. Rebek, Jr *J. Am. Chem. Soc*., 2008, **130**, 7810.

(27) C. J. Brown, R. G. Bergman and K. N. Raymond, *J. Am. Chem. Soc.*, 2009, **131**, 17530; C. J. Hastings, M. D. Pluth, R. G. Bergman and K. N. Raymond, *J. Am. Chem. Soc.*, 2010, **132**, 6938.

(28) R. Ballardini, G. Varani and V. Balzani, *J. Am. Chem. Soc.*, 1980, **102**, 1720; K. Maruyama, M. Muraoka and Y. Naruta, *J. Org. Chem.*, **1981**, *46*, 983; R. M. Wilson, S. W. Wunderly, T. F. Walsh, A. K. Musser, R. Outcalt, F. Geiser, S. K. Gee, W. Brabender, L. Yerino, Jr, T. T. Conrad and G. A. Tharp, *J. Am. Chem. Soc.*, 1982, **104**, 4429; K. A. Schnapp, R. M. Wilson and D. M. Ho, *J. Am. Chem. Soc.*, 1990, **112**, 3700; J.-H. Xu, Y.-L. Song, Z.-G. Zhang, L.-C. Wang and J.-W. Xu, *Tetrahedron* 1994, **50**, 1199; M. A. Ciufolini, M. A. Rivera-Fortin, V. Zuzukin and K. H. Whitmire, *J. Am. Chem. Soc.*, 1994, **116**, 1272; W. Wang, W.-J. Zhang, L. Wang, C. K. Quah, H.-K. Fun, J.-H. Xu and Y. Zhang, *J. Org. Chem.*, 2013, **78**, 6211.

(29) E. Paterno and G. Chieffi, *Gazz. Chim. Ital.*, 1909, **39**, 341; G. Büchi, C. G. Inman and E. S. Lipinsky, *J. Am. Chem. Soc.*, 1954, **76**, 4327; C. W. Funke and H. Cerfontain, *J. Chem. Soc., Perkin Trans. 2*, 1976, 1902; D. Bryce-Smith, E. H. Evans, A. Gilbert and H. S. McNeill, *J. Chem. Soc., Perkin Trans. 2*, 1991, 1587; T. Bach, K. Jödicke, K. Kather and R. Fröhlich, *J. Am. Chem. Soc.*, 1997, **119**, 2437; T. Bach, *Synthesis*, 1998, 683.

(30) D. Sun, S. M. Hubig and J. K. Kochi, *J. Org. Chem.*, 1999, **64**, 2250.

(31) K. Kokubo, T. Masaki and T. Oshima, *Org. Lett.*, 2000, **2**, 1979.

(32) A. Ikeda and S. Shinkai, *Chem. Rev.*, 1997, **97**, 1713.

(33) H. Grennberg, A. Gogoll and J.-E. Backvall, *Organometallics*, 1993, **12**, 1790; R. A. Klein, C. J. Elsevier and F. Hartl, *Organometallics*, 1997, **16**, 1284; J. A. Gonçalves and E. V. Gusevskaya, *Appl. Catal. A*, 2004, **258**, 93.

(34) M. J. S. Dewar, *Bull. Soc. Chim. Fr.*, 1951, **18**, C71; J. Chatt and L. A. Duncanson, *J. Chem. Soc.,* 1953, 2939; F. R. Hartley, *Chem. Rev.*, 1969, **69**, 799; H. Zhao, A. Ariafard and Z. Lin, *Inorg. Chim. Acta*, 2006, **359**, 3527.

(35) H. Minematsu, S. Takahashi and N. Hagihara, *J. Organomet. Chem.*, 1975, **91**, 389; M. Hiramatsu, K. Shiozaki, T. Fujinami and S. Sakai, *J. Organomet. Chem.*, 1983, **246**, 203.

(36) B. M. Trost, P. E. Strege, L. Weber, T. J. Fullerton and T. J. Dietsche, *J. Am. Chem. Soc.*, 1978, **100**, 3407; B. M. Trost and P. J. Metzner, *J. Am. Chem. Soc.*, 1980, **102**, 3572; H. Nakamura, H. Iwama and Y. Yamamoto, *J. Am. Chem. Soc.*, 1996, **118**, 6641.

(37) R. E. Wolf, Jr and S. R. Cooper, *J. Am. Chem. Soc.*, 1984, **106**, 4646; M. Delgado, R. E. Wolf, Jr, J. R. Hartman, G. McCafferty, R. Yagbasan, S. C. Rawle, D. J. Watkin and S. R. Cooper, *J. Am. Chem. Soc.*, 1992, **114**, 8983; T. D. Chung, D. Choi, S. K. Kang, S. K. Lee, S.-K. Chang and H. Kim, *J. Electroanal. Chem.*, 1995, **396**, 431; I. Ando, H. Miyake, Y. Ohki, K. Ujimoto and H. Kurihara, *Bull. Chem. Soc. Jpn.*, 2000, **73**, 2753.

(38) Y. Wang, J. Yuan, L. Wang and C. Hao, *J. Chem. Eng. Data*, 2010, **55**, 2233.

(39) Crystallographic data for the structure of $\mathbf{2aE_0}$ has been deposited with the Cambridge Crystallographic Data Center as supplementary publication numbers CCDC 894295.

(40) Oxidation potential of TME is almost consistent with the reported value (1.53 V vs SCE) in the following reference: Fox, M. A.; Chanon, M., Eds. *Photoinduced Electron Transfer*; Elsevier: Amsterdam, 1988.

(41) The W_p value is negligible in a polar MeCN solution.

(42) T. Itoh and R. Hashimoto, *J. Lumin.*, 2012, **132**, 236.

(43) J. Xue, J.-W. Xu, L. Yang and J.-H. Xu, *J. Org. Chem.*, 2000, **65**, 30.

(44) D. Bryce-Smith and A. Gilbert, *Tetrahedron Lett*., 1964, **47**, 3471; J.-H. Xu, Y.-L. Song, Z.-G. Zhang, L.-C. Wang and J.-W. Xu. *Tetrahedron*, 1994, **50**, 1199; G. Jones, II and W. A. Haney, *J. Phys. Chem*., 1986, **90**, 5410.

(45) DFT calculations were carried out using Gaussian 09. Geometry optimizations were performed for a single molecule in a gas phase.

(46) M. J. Frisch et al. Gaussian 09, Revision A.02, Gaussian, Inc.: Wallingford, CT, 2009 (Full author list is shown in SI).

(47) J. Yuasa, S. Yamada and S. Fukuzumi, *Chem.–Eur. J*., 2008, **14**, 1866.

(48) S. Fukuzumi, T. Suenobu, M. Patz, T. Hirasaka, S. Itoh, M. Fujitsuka and O. Ito, *J. Am. Chem. Soc*., 1998, **120**, 8060; S. Fukuzumi, K. Ohkubo, Y. Kawashima, D. S. Kim, J. S. Park, A. Jana, V. Lynch, D. Kim and J. L. Sessler, *J. Am. Chem. Soc*., 2011, **133**, 15938.

(49) B. S. Prabhananda, *J. Chem. Phys*., 1983, **79**, 5752.

(50) The WinSIM program is developed at the NIEHS by Duling (URL: http://www.niehs.nih.gov/research/resources/software/tools/index.cfm): D. R. J. Duling, *Magn. Res. Ser. B*, 1994, **104**, 105.